

Photocurrents Mechanisms And Performance Considerations Of A Reach Through P⁺-N-N⁺ Silicon Photodiode

L.Dr.Muneer Aboud Hashem
Electrical Engineering Department
College of Engineering
Al .Mustansiriya University

L. Fadhil Sahib Hasan
Electrical Engineering Department
College of Engineering
Al. Mustansiriya University

Abstract

The proposed model is a reverse-biased p⁺-n-n⁺ silicon photodiode which offers good quantum efficiency and high response speed suitable for photodetectors application. The theoretical analysis of the device is started with the evaluation of the built-in, reachthrough, and breakdown voltages. Photocurrent mechanisms theoretical treatment in each layer of the device are modeled. The effect of the surface recombination velocity and the absorption coefficient on the minority carries distribution in each layer within the device and on the overall device performance is presented. An effective and powerful modeling process of the mathematical foundations of the photodiode is performed with the aid of MATLAB R2008a version 6.5A. It is found that for a low reachthrough voltage, the concentration of the n layer should be reduced, the photocurrents increases as the width of the P⁺ and n layer increase at a relatively low surface recombination velocity and better absorption coefficient. A good quantum efficiency and high response speed of the photodiode in the wavelength region 0.5 μm - 0.82 μm can be achieved by considering an optimum values of the effecting parameters in the n key layer of the device.

Keywords: reachthrough voltage, photocurrent, quantum efficiency, photodiode.

الخلاصة

يتناول البحث نموذجاً مقترحاً للثنائي الضوئي السليكون p⁺-n-n⁺ ذو الانحياز العكسي . وهذا النموذج يقدم كفاءة كمية جيدة وسرعة استجابته عالية مناسبة لتطبيقات الكشف الضوئي . ان التحليل النظري للثنائي يبدأ من حساب فولتيات جهد الانتشار وجهد الوصول وجهد الانهيار. وقد تم نمذجة المعالجات الرياضية للتيارات الضوئية كما تم دراسة تأثير سرعة اعادة الاتحاد السطحية ومعامل الامتصاص على توزيع حاملات الشحنات الاقلية ومجمل كفاءة الثنائي في كل طبقة. وانجز النموذج الرياضي للثنائي الضوئي باستخدام MATLAB R2008a النسخة 6.5A بطريقة فعالة لتمثيل العلاقات الرياضية في مختلف طبقات الثنائي . وقد وجد انه لتقليل فولتية جهد الوصول يجب ان يكون تركيز عرض طبقة n وسرعة اعادة الاتحاد السطحية تأثير على كفاءة اداء الثنائي وباختيار قيم مثلثي يمكن الوصول الى اداء جيد وسريع في منطقة الاطوال الموجية 0.5μm-0.82μm .

Glossary of Symbols

A	device area
D_n	diffusion coefficient of electrons
D_p	diffusion coefficient of holes
E_c	critical field at breakdown
E'_c	critical field at the n-n ⁺ interface
E_{fn}	Fermi level in the n layer
E_{fn^+}	Fermi level in the n ⁺ layer
E_{in}	intrinsic Fermi level in the n layer
E_{in^+}	intrinsic Fermi level in the n ⁺ layer
E'_c	critical field at the n-n ⁺ interface
f	frequency of the photon
F_i	number of incident photons per square centimeter per second
G_n	generation rate of electrons on the p ⁺ layer
h	Plank's constant
K	Boltzmann's constant
L_n	diffusion lengths of electrons
L_p	diffusion length of holes
n_i	intrinsic concentration of silicon
n_{p^+}	minority carriers concentration
n_{p^+o}	minority carriers concentrations
N_n	majority carriers concentration of the n layer
N_{p^+}	majority carriers concentration of the p ⁺ layer
p_{n^+}	minority carriers concentration in the n ⁺ layer
p_{n^+o}	minority carriers concentration in the n ⁺ layer at thermal equilibrium

P_o	incident optical power
q	electronic charge
R	responsivity
S_n	surface recombination velocity of electrons
T	absolute temperature
V	reverse-bias voltage
V_{bi1}	built-in potential for an p^+ -n junction
V_{bi2}	the built-in potential for an n- n^+ junction
V_{BR}	breakdown voltage
V_{BRT}	reach through voltage
V_{RT}	reach through voltage
W_n	width of the n-layer
W_{p^+}	width of the p^+ layer
x	distance from the semiconductor surface to the p^+ -n junction
X_1	depletion layer width at the p^+ -n junction
X_2	depletion layer width at n- n^+ junction
α	absorption coefficient
ϵ_s	absolute permittivity
η	quantum efficiency
λ	wavelength of the incident photon
v_s	saturation velocity
τ_g	generation lifetime
τ_n	minority carriers lifetime of electrons
τ_p	minority carriers lifetime of holes

1- Introduction

Efficient and accurate models of optoelectronic devices such as laser diodes, light emitting diodes, and photodiodes are required for the design and development of high speed optoelectronic systems and circuits. High performance photodetectors for fast photodetection and microwave photonics applications are reported using compound semiconductors [1]-[3].

The proposed model, depicted in Fig. 1, is a p⁺-n-n⁺ silicon photodiode device with a uniform doping in each layer. The device is operated in a photoconductive mode and a typical photodiode material, silicon is used because of low dark current, high speed, and good sensitivity between roughly 400 and 1000nm^[4], the n layer is fully depleted for optimum quantum efficiency and frequency response. The energy band diagram of the device is depicted in Fig. 2. First, the built-in potential V_{bi1} for a step (abrupt) p⁺-n⁻ junction is given by [5]

$$V_{bi1} = \frac{KT}{q} \ln \frac{N_{p^+} N_n}{n_i^2} \quad (1)$$

where K is the Boltzmann's constant, T is the absolute temperature, q is the electronic charge, N_{p^+} is the concentration of the p⁺ layer, N_n is the concentration of the n layer, and n_i is the intrinsic concentration of silicon., second, the built-in potential V_{bi2} for an n-n⁺ junction can be evaluated from the difference in the position of the Fermi level in each layer. In the n layer [6]

$$E_{fn} = E_{in} - KT \ln \frac{N_n}{n_i} \quad (2)$$

where E_{fn} and E_{in} are the Fermi level and the intrinsic Fermi level in the n layer, respectively. Similarly for the n⁺ layer

$$E_{fn^+} = E_{in^+} - KT \ln \frac{N_{n^+}}{n_i} \quad (3)$$

where E_{fn^+} and E_{in^+} are the Fermi level and the intrinsic Fermi level, respectively. The concept of the constancy of the Fermi level under thermal equilibrium gives $E_{fn} = E_{fn^+}$. Hence,

$$E_{in} - KT \ln \frac{N_n}{n_i} = E_{in^+} - KT \ln \frac{N_{n^+}}{n_i} \quad (4)$$

Therefore, we have

$$E_{in+} - E_{in} = KT \ln \frac{N_{n+}}{N_n} = qV_{bi2} \quad (5)$$

So, the built-in potential V_{bi2} for an n-n⁺ junction is given by

$$V_{bi2} = \frac{KT}{q} \ln \frac{N_{n+}}{N_n} \quad (6)$$

which is very small $\approx 0.1V$ as compared with that at the first junction.

2- Reach Through and Breakdown Voltages

The model assumes the device is partitioned into a depletion region and a neutral region ^{[1]-[3]} so the electric field is constant in the neutral region. For a small reverse bias voltage, V applied to the device, the depletion layer widths X_1 and X_2 at the p⁺-n and n-n⁺ junctions, depicted in Fig. 3 ^[7], are given by

$$X_1 = \left[\frac{2\epsilon_s(V_{bi1} + V)}{qN_n} \right]^{1/2} \quad (7)$$

and

$$X_2 = \left[\frac{2\epsilon_s(V_{bi2} + V)}{qN_n} \right]^{1/2} \quad (8)$$

where ϵ_s is the absolute permittivity ^[8]. A reach through voltage, V_{RT} , is reached by further increasing in the reverse bias voltage as depicted in Fig. 4 and can be obtained from the condition

$$W_n = X_1 + X_2 \quad (9)$$

where W_n is the width of the n-layer. Eq. 9 can be written as

$$X_2^2 = W_n^2 - 2W_nX_1 + X_1^2 \quad (10)$$

Substituting of Eqs.7 and 8 into 9 gives

$$\frac{2\epsilon_s(V_{bi2} + V_{RT})}{qN_n} = W_n^2 - 2 \left[\frac{2\epsilon_s(V_{bi1} + V_{RT})}{qN_n} \right]^{1/2} W_n + \frac{2\epsilon_s(V_{bi1} + V_{RT})}{qN_n} \quad (11)$$

Thus,

$$V_{RT} = \frac{qN_n W_n^2}{8\epsilon_s} + \frac{\epsilon_s (V_{bi1} - V_{bi2})^2}{2qN_n W_n^2} + \frac{(V_{bi1} - V_{bi2})}{2} - V_{bi1} \quad (12)$$

The reach through voltage versus the width of the n⁻ layer is depicted in Fig. 5 with the aid of MATLAB numeric computation software [9], it can be seen that as the width of the n⁻ layer increases, a reach through voltage of the photodiode increases but it decreases with the decrease of the carriers concentration for a given width of the n⁻ layer. It is interesting to calculate the breakdown voltage V_{BRT} for the reach through device. Here, for lightly doped concentration in the n⁻ layer and the width of this layer is small compared with the width W_{BRT} at breakdown as depicted in Fig. 4, the breakdown voltage, V_{BR} , can be calculated from the solution of the Poisson's equation for the case of a step junction and is given by

$$V_{BR} = \frac{\epsilon_s E_c^2}{2qN_n} \quad (13)$$

where E_c is the critical field at breakdown which can be evaluated from the relation between E_c and N_n . From Fig. 4

$$\text{slop AB} = \text{slop BC} \quad (14)$$

$$\frac{-E_c + E'_c}{-W_n} = \frac{-E'_c}{W_n - W_{BRT}} \quad (15)$$

where E'_c is the critical field at the n-n⁺ interface. So,

$$\frac{E'_c}{E_c} = 1 - \frac{W_n}{W_{BRT}} \quad (16)$$

and

$$\frac{V_{BRT}}{V_{BR}} = \frac{-E'_c W_n + (-E_c + E'_c) W_n / 2}{-W_{BRT} E_c / 2} \quad (17)$$

From Eqs. 16 and 17

$$\frac{V_{BRT}}{V_{BR}} = \frac{2W_n}{W_{BRT}} - \frac{W_n^2}{W_{BRT}^2} \quad (18)$$

The breakdown voltage of the device against the width of the n⁻ layer is plotted in Fig. 6 and it increases as the width of this layer is increased since at fixed concentration the critical field at breakdown is not changed and hence V_{BR} and W_{BRT} remain constants.

3- Photocurrents Analysis

When a monochromatic light is incident on the p^+ layer, the generation rate of electrons, G_n , is given by

$$G_n = F_i \alpha e^{-\alpha x} \tag{19}$$

where α is the absorption coefficient which is a function of photon energy^[10], x is the distance from the semiconductor surface to the p^+ -n junction, and F_i is the number of incident photons per square centimeter per second given by

$$F_i = \frac{P_o}{Ahf} \tag{20}$$

where P_o is the incident optical power, A is the device area, h is the plank's constant, and f is the frequency of the photon. The continuity equation for p^+ layer under low injection level is given by

$$D_n \frac{d^2 n_{p+}}{dx^2} - \frac{n_{p+} - n_{p+o}}{\tau_n} + G_n = 0 \tag{21}$$

where D_n is the diffusion coefficient of electrons, n_{p+} is the minority carriers concentration, n_{p+o} is the minority carriers concentrations at thermal equilibrium, and τ_n is the minority carriers lifetime. The general solution of this second order differential equation is given by^[11]

$$n_{p+} - n_{p+o} = K_1 \cosh(x/L_n) + K_2 \sinh(x/L_n) - F_i \alpha e^{-\alpha x} \tag{22}$$

where L_n is the diffusion lengths of electrons given by

$$L_n = (D_n \tau_n)^{1/2} \tag{23}$$

and K_1, K_2 are constants of integration given by

$$K_1 = \frac{\alpha F_i \tau_n}{\alpha^2 L_n^2 - 1} \left[\frac{(C_1 + \alpha L_n) \sinh(W_{p+}/L_n) + e^{-\alpha W_{p+}}}{C_1 \sinh(W_{p+}/L_n) + \cosh(W_{p+}/L_n)} \right] \tag{24}$$

and

$$K_2 = \frac{\alpha F_i \tau_n}{\alpha^2 L_n^2 - 1} \left[\frac{C_1 e^{-\alpha W_{p+}} - (C_1 + \alpha L_n) \cosh(W_{p+}/L_n)}{C_1 \sinh(W_{p+}/L_n) + \cosh(W_{p+}/L_n)} \right] \tag{25}$$

$$C_1 = S_n L_n / D_n \tag{26}$$

where W_{p+} is the width of the p^+ layer and S_n is the surface recombination velocity. Substituting of Eqs, 24 and 25 into Eq.22 gives

$$n_{p+} - n_{p+o} = \frac{\alpha F_i \tau_n}{\alpha^2 L_n^2 - 1} \left[\frac{(C_1 + \alpha L_n) \sinh(W_{p+} - x/L_n) + e^{-\alpha W_{p+}} \{ \sinh(x/L_n) + \cosh(x/L_n) \}}{C_1 \sinh(W_{p+}/L_n) + \cosh(W_{p+}/L_n)} - e^{-\alpha x} \right] \tag{27}$$

the resulting photocurrent density is given by

$$J_{p+} = q D_n \frac{dn_{p+}}{dx} = - \frac{q \alpha F_i L_n}{\alpha^2 L_n^2 - 1} \left[\frac{(C_1 + \alpha L_n) \sinh(W_{p+} - x/L_n) - e^{-\alpha W_{p+}} \{ \sinh(x/L_n) + \cosh(x/L_n) \}}{C_1 \sinh(W_{p+}/L_n) + \cosh(W_{p+}/L_n)} - \alpha L_n e^{-\alpha x} \right] \tag{28}$$

and the photocurrent density at $x = W_{p+}$ is given by

$$= - \frac{q \alpha F_i L_n}{\alpha^2 L_n^2 - 1} \left[\frac{(C_1 + \alpha L_n) - e^{-\alpha W_{p+}} \{ C_1 \cosh(W_{p+}/L_n) + \sinh(W_{p+}/L_n) \}}{C_1 \sinh(W_{p+}/L_n) + \cosh(W_{p+}/L_n)} - \alpha L_n e^{-\alpha W_{p+}} \right] \tag{29}$$

The minority carrier distribution versus the width of the p^+ layer is depicted in Figs. 7 and 8, respectively. From the observation of these figures, it can be seen that the minority carriers decay as we move toward the depletion region and it is affected with both the surface recombination velocity and the absorption coefficient that is strong dependent on the wavelength of the incident light. Here, it increases with the decrease in the surface recombination velocity and with the increase of the absorption coefficient. The same is true for the photocurrent density as depicted in Figs. 9 and 10, respectively.

The high electric field in the depletion region accelerates the carriers outside the depletion region; the photocurrent density due to these carriers in the depletion region is given by

$$J_{n-} = -q \int_{W_{p+}}^{W_{p+} + W_n} \alpha F_i e^{-\alpha x} dx = -q F_i \left[e^{-\alpha W_{p+}} - e^{-\alpha(W_{p+} + W_n)} \right] + \frac{q n_i W_n}{\tau_g} \tag{30}$$

where τ_g is the generation lifetime. The second term in Eq. 30 is small and can be neglected. The carriers in the depletion region also contribute to the total photocurrent that it increases with the increase in the absorption coefficient for a given width of the n layers as seen from

the relation depicted in Fig. 11. Following the same procedure for the p^+ layer above, the minority carrier distribution and the photocurrent density in the n^+ layer is given by

$$p_{n+} - p_{n+o} = \left(-p_{n+o} + \frac{\alpha F_i \tau_p}{\alpha^2 L_p^2 - 1} e^{-\alpha W_n} \right) e^{\frac{W_n - x}{L_p}} - \frac{\alpha F_i \tau_p}{\alpha^2 L_p^2 - 1} e^{-\alpha x} \quad (31)$$

and

$$J_{n+} = \frac{qD_p}{L_p} \left(-p_{n+o} + \frac{\alpha F_i \tau_p}{\alpha^2 L_p^2 - 1} e^{-\alpha W_n} \right) e^{\frac{W_n - x}{L_p}} - q\alpha D_p \frac{\alpha F_i \tau_p}{\alpha^2 L_p^2 - 1} e^{-\alpha x} \quad (32)$$

The photocurrent density at $x = W_n$ is given by

$$J_{n+} = -\frac{qL_p p_{n+o}}{\tau_p} - \frac{qF_i \alpha L_p^2}{1 + \alpha L_p} e^{-\alpha W_n} \quad (33)$$

where p_{n+} and p_{n+o} are the minority carriers concentration and minority carriers concentration at thermal equilibrium, respectively, L_p is the diffusion length of holes, D_p is the diffusion coefficient of holes, and τ_p is the minority carriers lifetime. The first term in Eq. 33 is small and can be neglected. As we move away from the depletion region the minority carriers and the photocurrent are decreased with the decrease of the absorption coefficient as depicted in Figs. 12 and 13, respectively.

4- Quantum Efficiency and Response Speed

The quantum efficiency, as it is well known, the number of electron-hole pairs generated per incident photon

$$\eta = \frac{J_{p+} + J_n + J_{n+}}{qF_i} \quad (34)$$

A responsivity, related to quantum efficiency is

$$R = \frac{\eta q}{h\nu} = \frac{\eta \lambda (\mu\text{m})}{1.24} \quad (35)$$

where λ is the wavelength of the incident photon, the absorption coefficient is an important factor that determine the quantum efficiency and it is a function of wavelength. The quantum efficiency is small at short wavelengths because although the value of α is very large, the penetration depth $1/\alpha$ is small and the radiation absorbs near the surface where the surface recombination velocity encountered and the recombination time is short, the photocarriers

will recombine before they are collected. In the large wavelength region where the large penetration depth, the quantum efficiency is also small despite of the contribution of the diffusion currents in the p^+ and n^+ region because of the small absorption coefficient.

However, a reasonable width of fully depleted n layer and better surface recombination velocity as a result of advance device process, a good quantum efficiency of the photodiode can be obtained in the wavelength region $0.5 \mu\text{m} - 0.82 \mu\text{m}$. The quantum efficiency as depicted in Figs. 14 and 15, respectively, because of the generation of the photocarriers is within the depletion region. The high electric field in the depletion region serves to sweep the photogenerated carriers and the carriers will drift at their saturation velocity, v_s . Another factors that affected the quantum efficiency of silicon photodiode is the reflectivity^[12], and in the device theoretical analysis model a good reflectivity is assumed.

The response speed of the device is affected with the width of the depletion region and should not be too high for high speed operation and is affected by the junction capacitance which arises as the length of the depletion region decreases, and this gives rise to the time constant of the device. The response speed of the device is given by

$$t_{tr} = \frac{W_n}{v_s} \quad (36)$$

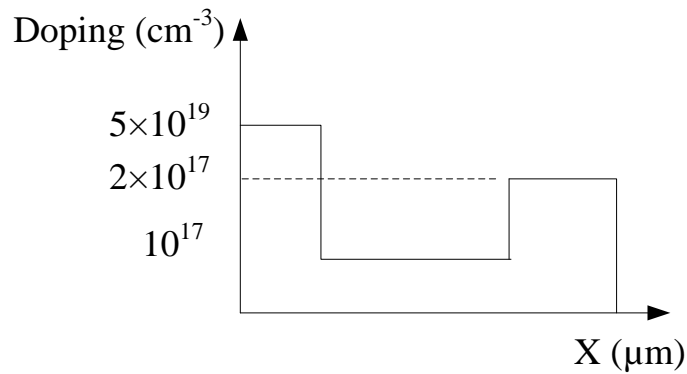
5- Computer Programming and Results

The software implementation of the theoretical treatment and relations of the photodiode are executed with the MATLAB R2008a version 6.5A powerful programming system with high accuracy and less complexity. The computer programming which realizes the relations between the reachthrough and breakdown voltages, minority carriers distribution, photocurrents density distribution, and quantum efficiency and different device parameters is presented by assigning a numeric values to a carriers concentrations, layer widths, surface recombination velocities and absorption coefficients to study the effects of these parameters on the device performance.

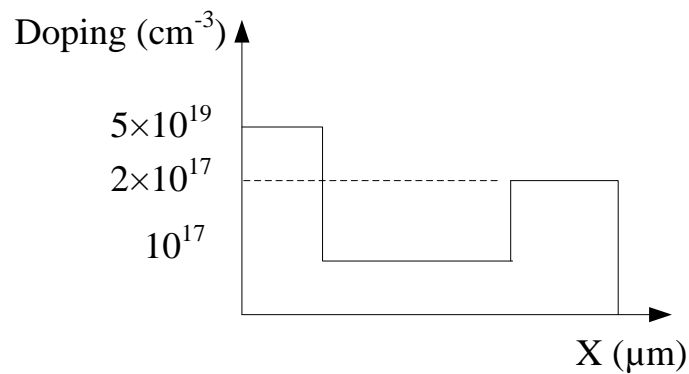
6- Conclusions and Discussions

The relations introduced in Figs. 1 to 15 between the device parameters stated that to minimize the reachthrough voltage a moderate doping and a small width of the n-layer is preferred. With this width of the depletion region, a high speed operation of the photodiode is achieved but this affect the quantum efficiency of the device so a tradeoff should be made between them. The minority carriers distribution in the p^+ layer is affected on both the surface recombination velocity and the absorption coefficient, hence, the photocurrent within the layer a minimum recombination velocity and a higher absorption coefficient are required. However, this photocurrent is small compared with that in the n-layer and does not significantly affect the overall device performance. The absorption coefficient affects the photocurrents density in the n- and n^+ layer, respectively and with a certain moderate value of

this coefficient the photocurrent increases as the width of the n-layer increased but this affects the response speed of the device. The quantum efficiency is strong dependence on the wavelength and a good quantum efficiency can be achieved with minimum surface recombination velocity and higher depletion region width.



(a)



(b)

Fig. 1 : P⁺-N-N⁺ Uniformly Doped Silicon Photodiode; (A) Device Structure; (B) Doping Profile.

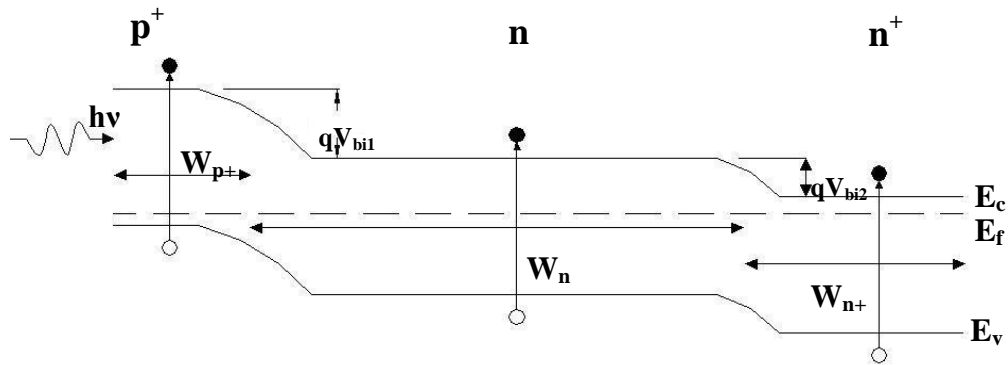


Fig. 2 Energy Band Diagram Of P⁺-N-N⁺ Silicon Photodiode.

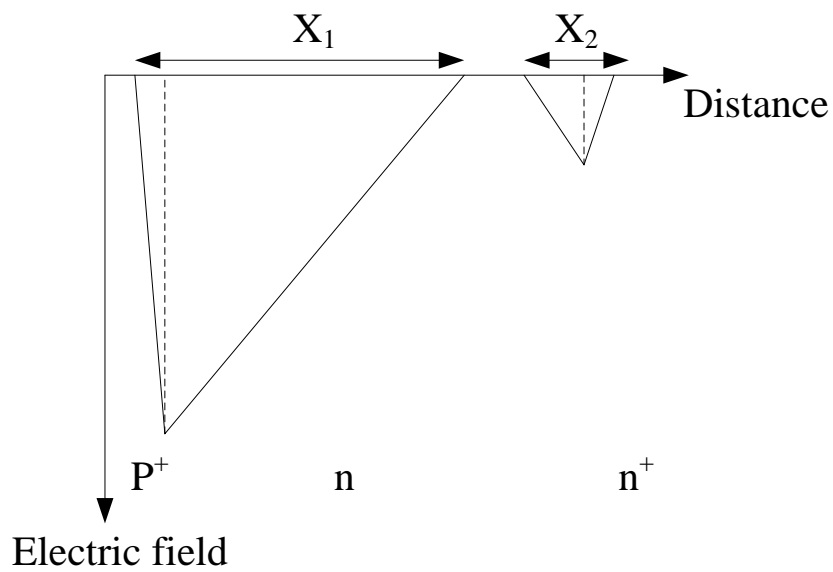


Fig. 3 Electric Field Distribution Within The P⁺-N-N⁺ Silicon Photodiode.

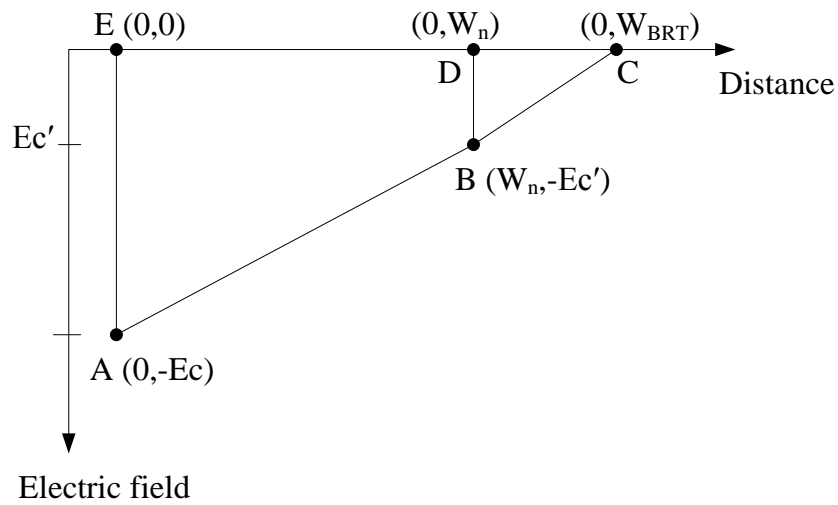


Fig. 4 Electric Field Distribution At Punch Through Voltage^[5].

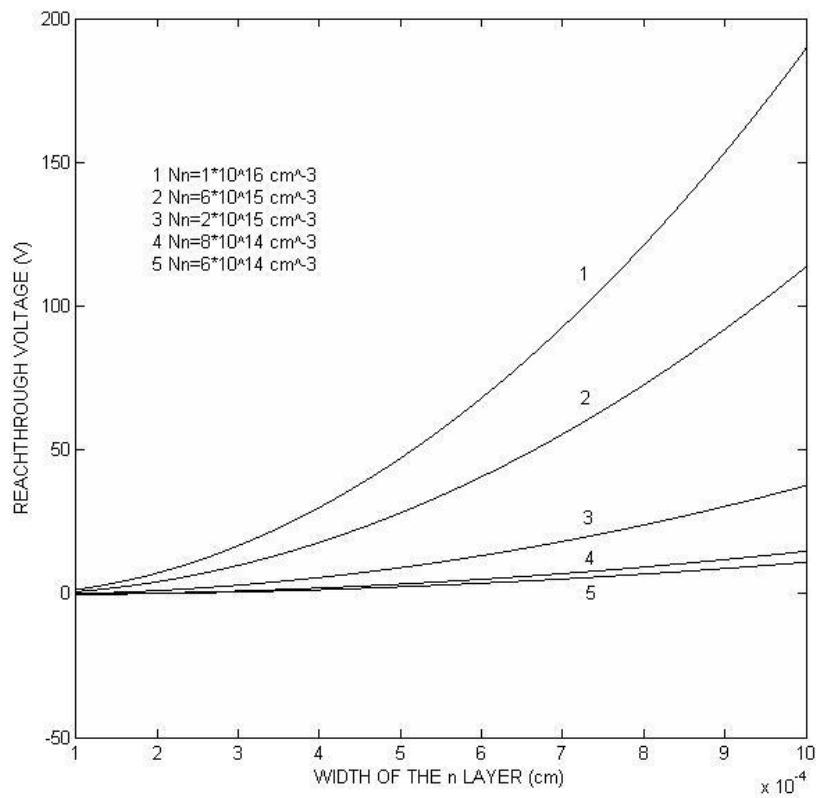


Fig. 5 Reachthrough Voltage Against The Width Of The N Layer For Different Carriers. Concentrations.

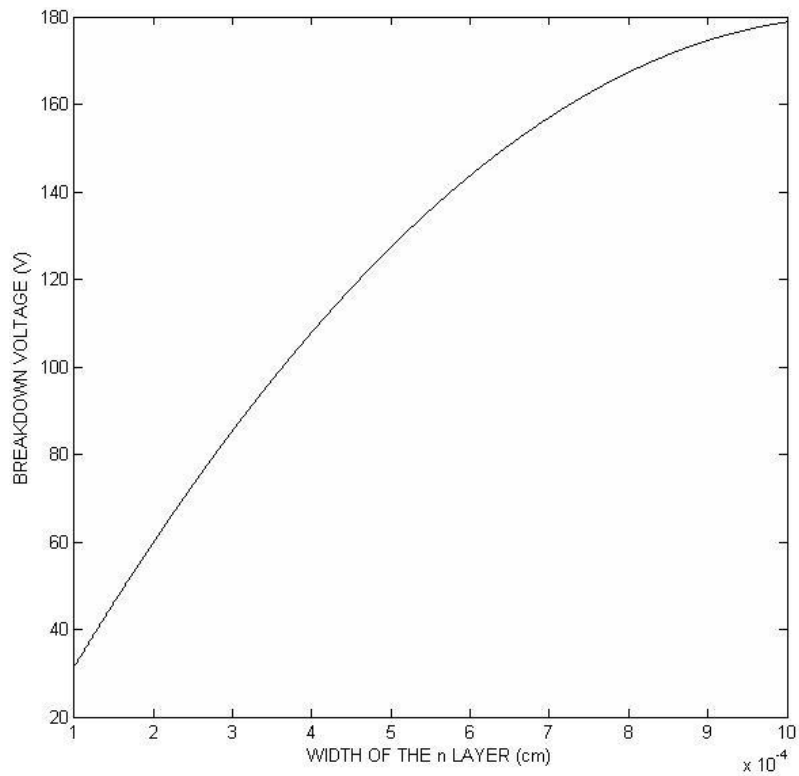


Fig. 6 : Breakdown Voltage As A Function Of The Depletion Width.

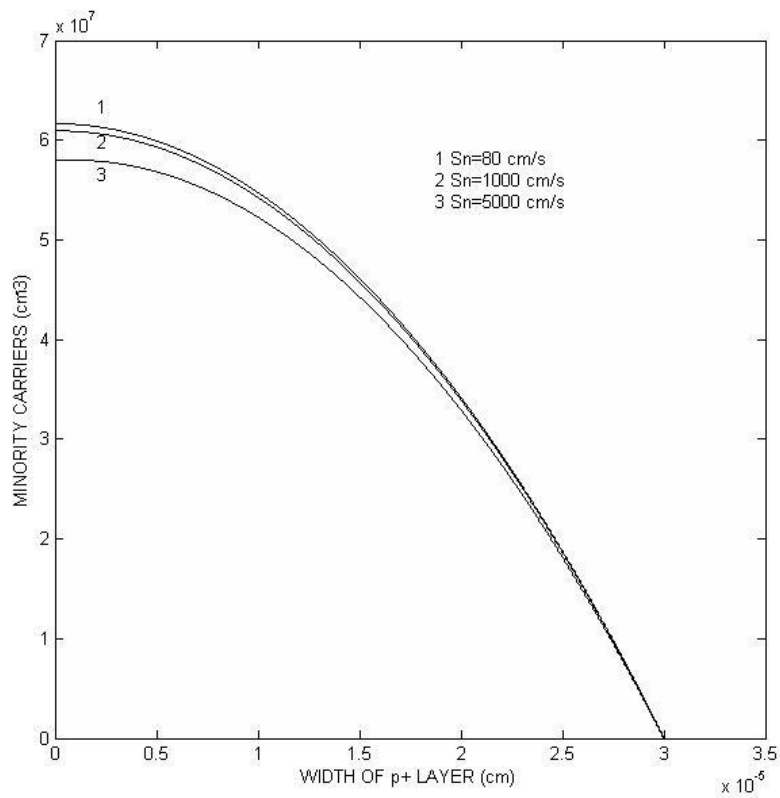


Fig. 7 : Minority Carriers Distribution In The P⁺ Layer For Different Surface Recombination Velocities.

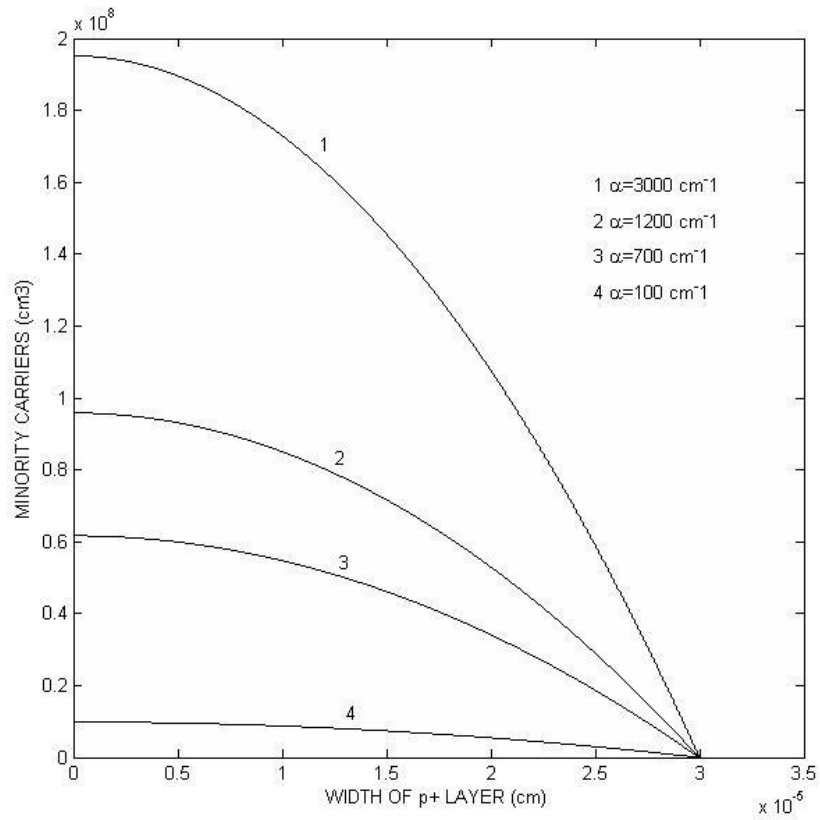


Fig. 8 Minority Carriers Distribution In The P⁺ Layer For Different Absorption Coefficients.

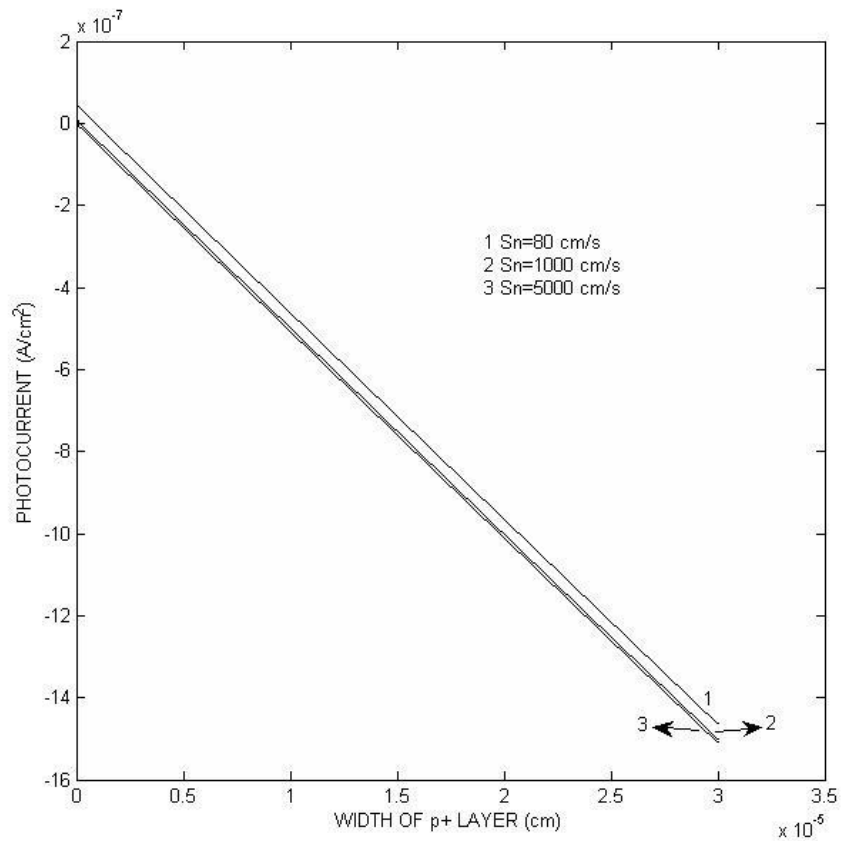


Fig. 9 Photocurrent density versus the width of the p⁺ layer for different surface recombination velocities.

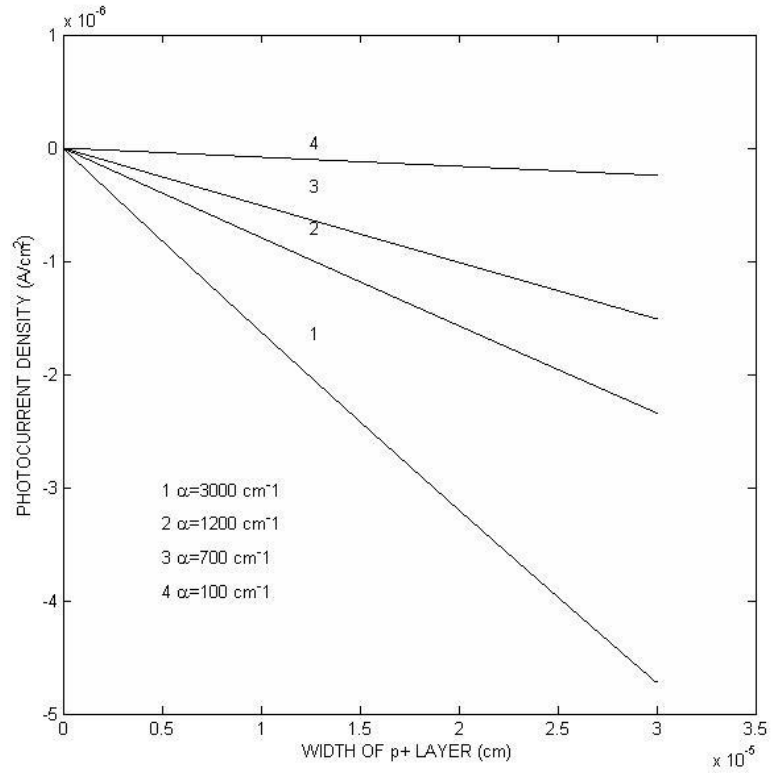


Fig. 10 Photocurrent density versus the width of the p⁺ layer for different absorption coefficients.

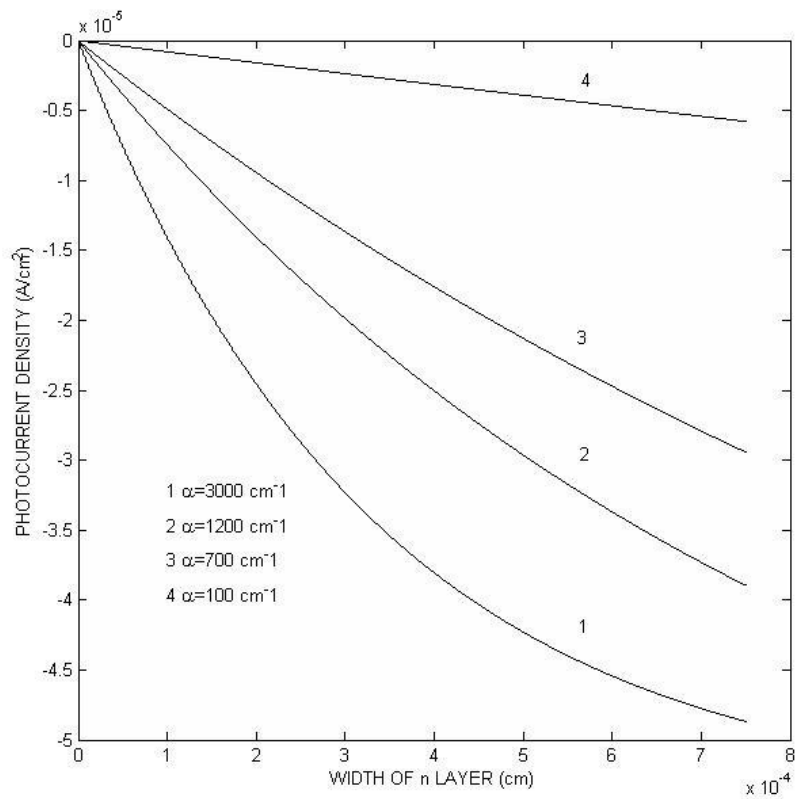


Fig. 11 Photocurrent density versus the width of the n layer for different absorption coefficients.

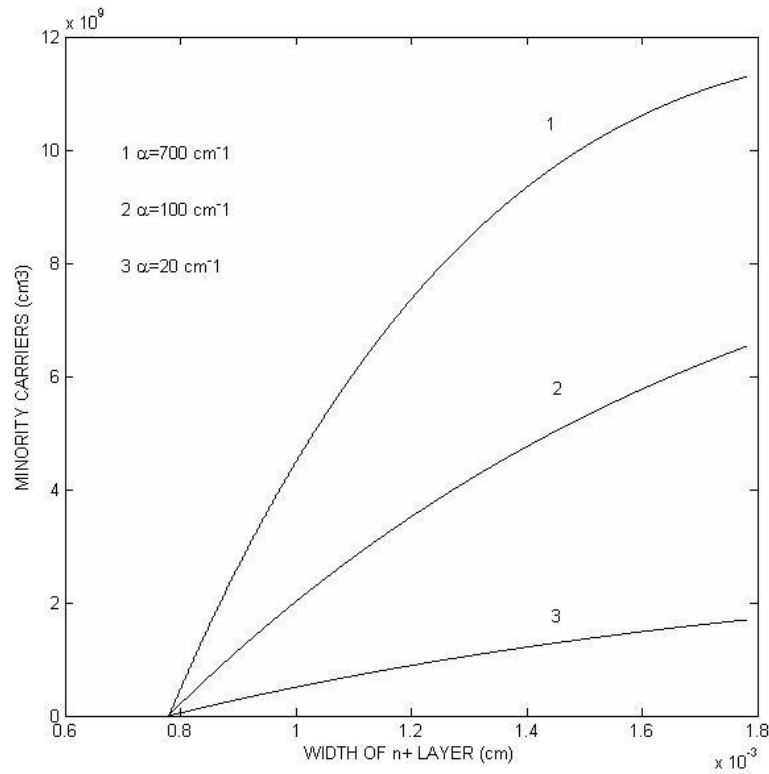


Fig. 12 minority carriers distribution in the n^+ layer for different absorption coefficients.

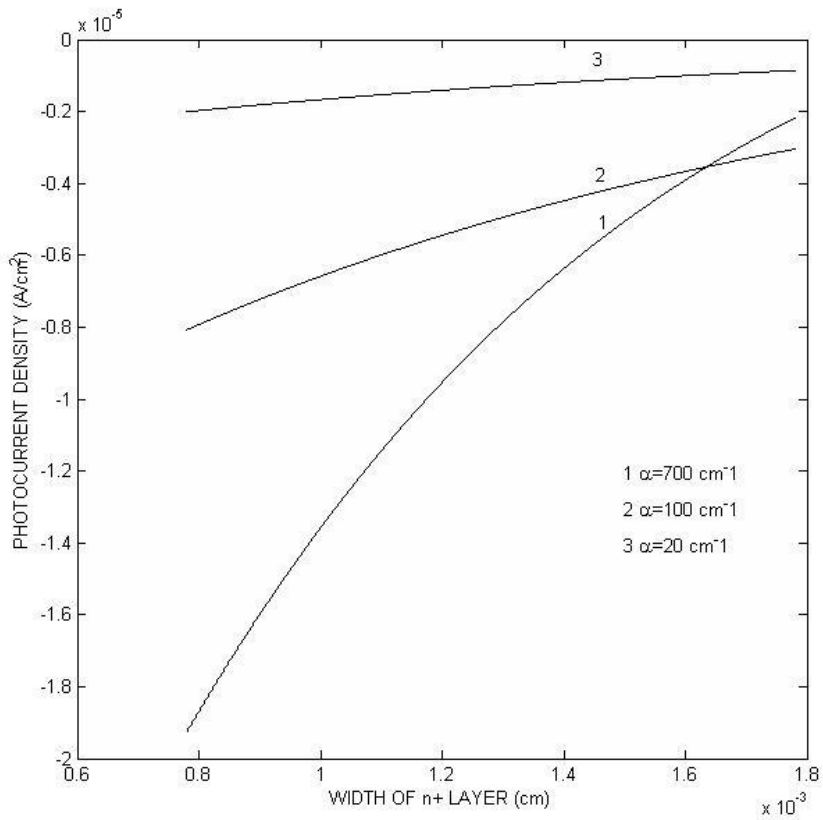


Fig. 13 Photocurrent density versus the width of the n^+ layer for different absorption coefficients.

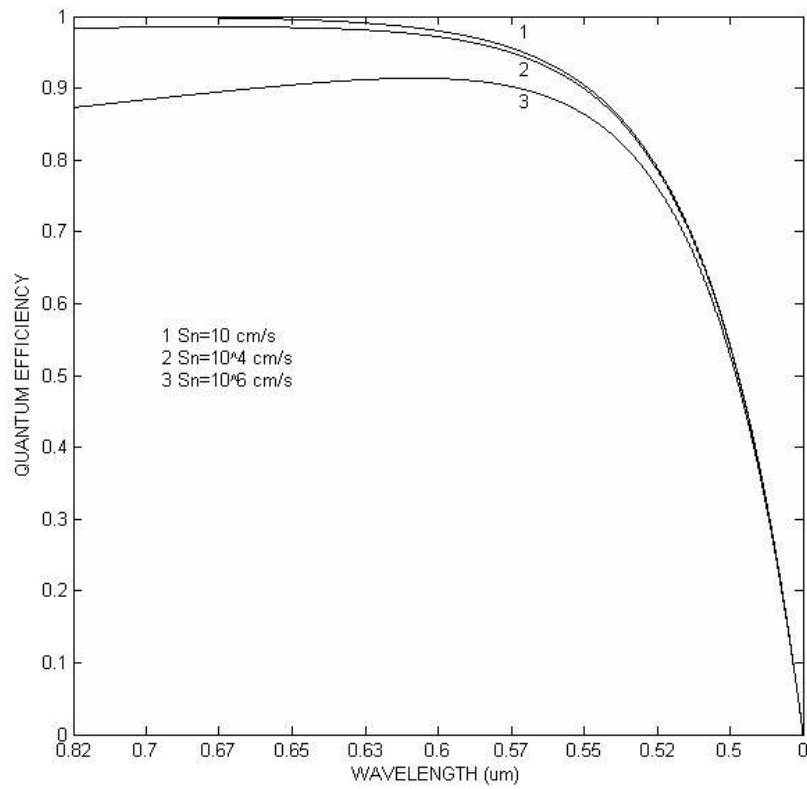


Fig. 14 Quantum efficiency as a function of surface recombination velocities.

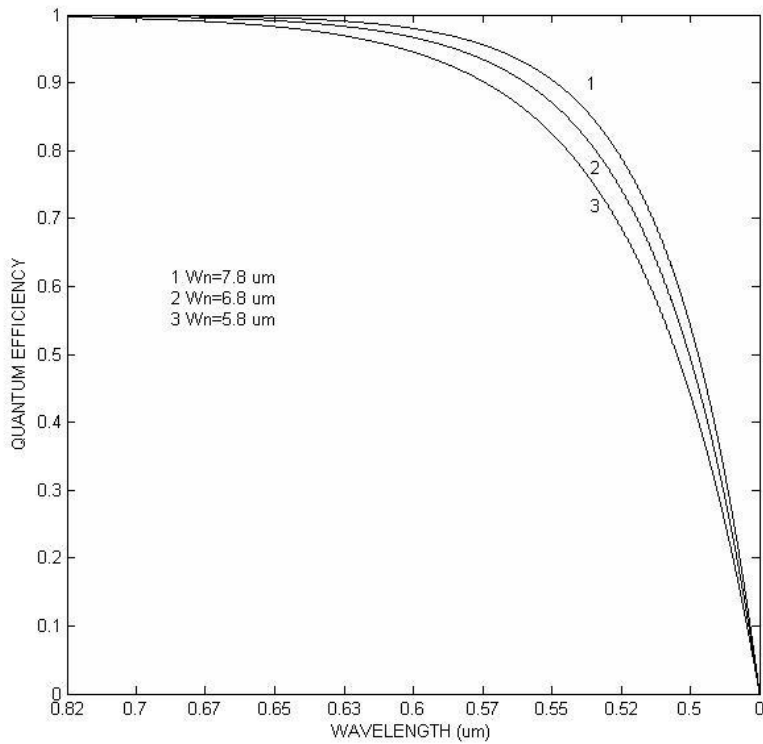
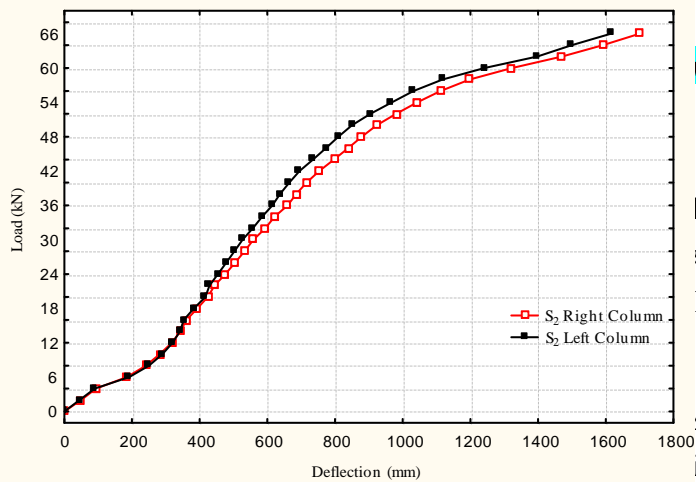


Fig. 15 Quantum efficiency for different depletion widths.



li, Bayram Butun, Orhan Aytur, Selim Unlu, and *and High-Performance p-i-n Photodiodes*," IEEE I.14. No.3, March 2002.

Y.C.Zhu, T.J.J. Kawaspen, E.A.J.M. Bente, F.H. *Modelling and characterization of InP-based high-* in Symposium IEEE/LEOS Benelux Chapter, 2003,

Enschede.

3. Sergei Malyshev, Alexander Chizh, and Vatslav Andrievski, " *InGaAs p-i-n Photodiodes for Microwave Applications*," 12th GAAS[®] Symposium-Amestrdam, 2004.
4. Rüdinger Paschotta," *Encyclopedia of Laser Physics and Technology*," <http://www.rp-photonics.com/photodiodes.html>, 2009.
5. S.M. Sze , " *Semiconductor Devices , Physics and Technology* , " John Wiley & sons, 1985 .
6. E.S.Yang," *Microelectronic Devices* , " McGraw Hill, Inc 1988.
7. J.Wilson and J.F.B.Hawkes," *Optoelectronics: An Introduction* , " Prentice-Hall Inc, 1983.
8. D.A.Neamen , " *Semiconductor Physics and Devices: Basic Principles* , " McGraw Hill, 2003.
9. John O. Attia, " *Electronics and Circuit Analysis Using MATLAB*," CRC Press,LLC 1999.
10. M.Melchior," *Demodulation and Photodetection Techniques*," in F.T. Arecchiand E.o. Schulz-Dubois,Eds., *Laser Handbook*,Vol.1,North-Holland,Amesterdam, pp725-835, 1972.
11. James R.Brannan and William E.Boyce, " *Differential Equations : An Introduction to Modern Methods and Applications*," John Wiley and Sons, Inc.2007.
12. Chris Hicks, Mark Kalatsky, Richard A. Metzler, and Alexander O. Goushcha, " *Quantum Efficiency of Silicon Photodiodes in the Near-Infrared Spectral Range*," Appl. Opt. **42**, 4415-4422, 2003.